ACADEMIC PRESS

Available online at www.sciencedirect.com

SCIENCE DIRECT®

Journal of Sound and Vibration 262 (2003) 1073–1090

JOURNAL OF SOUND AND VIBRATION

www.elsevier.com/locate/jsvi

Bending vibrations of wedge beams with any number of point masses

Jong-Shyong Wu[a,*], Der-Wei Chen[b]

[a] *Department of Naval Architecture and Marine Engineering, National Chen-Kung University, Tainan 701, Taiwan, ROC*
[b] *Department of Naval Architecture, Chung-Cheng Institute of Technology, Ta-Shi 335, Taiwan, ROC*

Received 16 August 2001; accepted 24 June 2002

Abstract

The natural frequencies and mode shapes of beams with constant width and linearly tapered depth (or thickness) carrying any number of point masses at arbitrary positions along the length of the beams were investigated using the Euler–Bernoulli equation. Use of the closed-form (exact) solutions for the natural frequencies and mode shapes of the unconstrained single-tapered beam (without carrying any point masses) and incorporation of the expansion theorem, the equation of motion for the associated constrained beam (carrying any point masses) were derived. Solution of the last equation will yield the desired natural frequencies and mode shapes of the constrained single-tapered beam. The bending vibrations of a single-tapered beam with six kinds of boundary conditions were investigated. Comparison with the existing literature or the traditional finite element method results reveals that the adopted approach has excellent accuracy and simple algorithm.
© 2002 Elsevier Science Ltd. All rights reserved.

1. Introduction

In this paper, for convenience, as in the existing literature, a beam is called "constrained" beam if it carries any concentrated point masses and is called "unconstrained" beam if it has no attachments. The literature relating to the vibration analysis of the non-uniform unconstrained beams is plenty [1–16]; however, the information regarding the dynamic behavior of the non-uniform constrained beams (carrying multiple concentrated elements) is relatively fewer [3,17–26]. All the statements of this paper refer to the Euler–Bernoulli beams unless particularly mentioned.

*Corresponding author. Fax: 886-6-2808458.
E-mail address: jswu@mail.ncku.edu.tw (J.-S. Wu).

0022-460X/03/$ - see front matter © 2002 Elsevier Science Ltd. All rights reserved.
PII: S0022-460X(02)01084-2

For the unconstrained non-uniform beams, Cranch and Adler [1] presented the closed-form solutions (in terms of the Bessel functions and/or power series) for the natural frequencies and mode shapes of complete beams with four kinds of rectangular cross-sections: linear depth $\times$ any power width, quadratic depth $\times$ any power width, cubic depth $\times$ any power width, and constant depth $\times$ any exponential width. Conway and Dubil [2] obtained similar closed-form solutions for the truncated-cone beams and the truncated-wedge beams. Goel [3] obtained the closed-form solutions of the single- and double-tapered truncated beams with non-idealized end conditions: spring hinged with rotational springs or tip mass. Housner and Keightley [4] solved a similar problem numerically with Myklestad–Prohl (MP) method and the Stodola (ST) method. Heidebrecht [5] determined the approximate natural frequencies and mode shapes of a non-uniform simply supported beam from the frequency equation and a Fourier sine series, where the frequency equation was derived from the Lagrangian equation by expanding the sectional mass $\bar{m}(x)$ and moment of inertia $I(x)$ of the beam in terms of the Fourier cosine series. Similar to Heidebrecht [5], Mabie and Rogers [6] used the second- and fourth order polynomials of axial co-ordinate $\boldsymbol{x}$ to express the sectional area $A(x)$ and moment of inertia $I(x)$, respectively, but they transformed the partial differential equation of free vibration of a double-tapered beam into the ordinary one, and then solved the last equation to get the natural frequencies. Downs [7] presented the natural frequencies and parts of the corresponding mode shapes of the cantilever beams with 36 combinations of linear depth and breadth taper based on both Euler and Timoshenko theories by using the dynamic discretization technique. Bailey [8] determined the natural frequencies of the non-uniform cantilever beams numerically by directly solving the frequency equation derived from the Hamilton's law. Gupta [9] derived the stiffness and consistent mass matrices for the linearly tapered beam element and then determined the natural frequencies and mode shapes of the tapered beams with the traditional finite element procedure. Naguleswaran determined the approximate natural frequencies of the single-tapered beams [10] and double-tapered beams [11] with a direct solution of the mode shape equation based on the Frobenius method. Abrate [12] found that the equation of motion of a non-uniform beam may be transformed into that of a uniform beam and then solved for the natural frequencies and mode shapes if the sectional area $A(x)$ and the moment of inertia $I(x)$ take the special forms. Laura et al. [13] investigated the natural frequencies of Bernoulli beams with constant width and bilinearly varying thickness using three well-known approximate numerical approaches: Rayleigh–Ritz method, differential quadrature method and finite element method. Datta and Sil [14] employed the reverse procedures of Ref. [1] to determine the natural frequencies of cantilever beams with constant width and linearly varying depth. Hoffmann and Wertheimer [15] presented a simple formula for determining the fundamental frequency of tapered cantilever beams with linear tapers as a function of the first-mode-deflection beam stiffness, the beam mass and a mass distribution parameter. Mabie and Rogers [16] studied the transverse vibration of single-tapered clamped–hinged beams.

For the natural frequencies and mode shapes of the non-uniform (constrained) beams carrying concentrated attachments at one end or both ends [17–22], the solution procedures are exactly the same as those for the non-uniform unconstrained beams [1–16]. The only difference is to change the boundary conditions for the unconstrained beams to accommodate the effects of the attachments at one end or both ends of the constrained beams, such as the restoring force due to translational spring, restoring bending moment due to rotational spring and inertial force due to

lumped mass and/or inertia moment due to concentrated mass moment of inertia. Because the problem becomes much complicated and intractable if the attachments are located at arbitrary positions along the length of the beam [23–26], the literature in this aspect is fewer, particularly for the cases with more than two intermediate attachments.

In Ref. [27], it has been found that the analytical and numerical, combined, method (ANCM) can deal with the foregoing drawback of the existing approaches. Hence this paper tries to use ANCM to tackle the title problem. First, the closed-form solutions for the natural frequencies and mode shapes of an unconstrained tapered beam with prescribed boundary conditions were determined analytically. Secondly, the equation of motion and the eigenvalue equation for the corresponding constrained tapered beam (carrying any number of point masses) were derived using the expansion theorem and the last natural frequencies and mode shapes. Finally, the eigenvalue equation was solved numerically to give the natural frequencies and mode shapes of the constrained tapered beam. The free vibration characteristic of a single-tapered beam with six boundary conditions was investigated. To validate the numerical results of ANCM, the traditional finite element method (FEM) was also used to solve the same problem and good agreement between the corresponding results was achieved.

2. Natural frequencies and normal mode shapes of an unconstrained wedge beam

For an unconstrained non-uniform Euler–Bernoulli beam as shown in Fig. 1, the equation of motion is given by [1–3]

$$\frac{\partial^2}{\partial x^2}\left(EI(x)\frac{\partial^2 y(x,t)}{\partial x^2}\right)+\rho A(x)\frac{\partial^2 y(x,t)}{\partial t^2}=0, \tag{1}$$

where x is the axial co-ordinate, y is the transverse deflection, E is Young's modulus, ρ is the mass density of material, $A(x)$ is the cross-sectional area of beam, $I(x)$ is the moment of inertia of $A(x)$ and t is time.

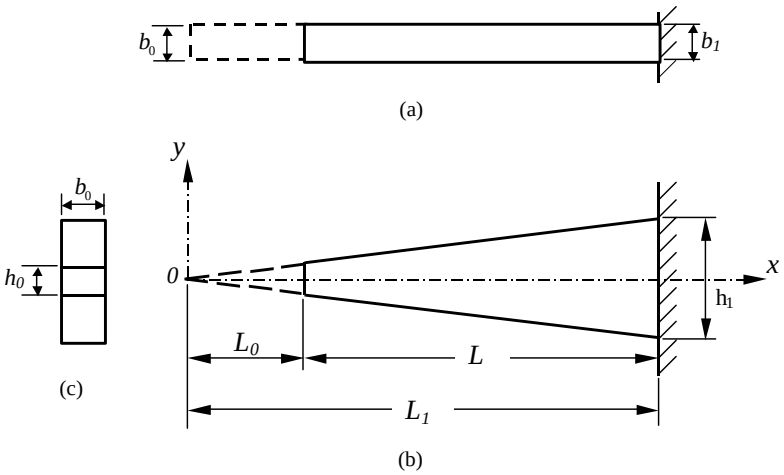

Fig. 1. Sketch for the wedge beam studied: (a) top view; (b) front view; (c) left side view.

For harmonic free vibration, one has

$$y(x,t) = W(x)e^{i\omega t}, \tag{2}$$

where $W(x)$ is the amplitude of the deflection $y(x,t)$ and represents the mode shape of the beam in free vibration, ω is the natural frequency and $i = \sqrt{-1}$. From Eqs. (1) and (2) one has

$$\frac{d^2}{dx^2}\left[EI(x)\frac{d^2W(x)}{dx^2}\right] - \rho A(x)\omega^2 W(x) = 0. \tag{3}$$

If the values of $\rho A(x)$ and $EI(x)$ appearing in Eq. (3) take the forms

$$\rho A(x) = \rho A_1\left(\frac{x}{L_1}\right)^n \quad \text{and} \quad EI(x) = EI_1\left(\frac{x}{L_1}\right)^{n+2} \tag{4a, b}$$

or

$$\rho A(\xi) = \rho A_1 \xi^n \quad \text{and} \quad EI(\xi) = EI_1 \xi^{n+2} \tag{5a, b}$$

with

$$\xi = \frac{x}{L_1}, \tag{6}$$

then the solution of Eq. (3) is given by [28–31]

$$W(\xi) = L_1^{-n/2}\xi^{-n/2}[c_1 J_n(z) + c_2 Y_n(z) + c_3 I_n(z) + c_4 K_n(z)]. \tag{7}$$

In Eqs. (4)–(6), L_1 is the length of the tapered beam from the sharp end (i.e., the origin of the axial co-ordinate x) to the large end, and

$$A_1 = b_1 h_1, \quad I_1 = \frac{b_1 h_1^3}{12} \tag{8a, b}$$

are, respectively, the cross-sectional area and moment of inertia of the beam at the large end, while n is a parameter defining variations of $A(x)$ and $I(x)$ along the length of the beam. In Eq. (7), J_n and Y_n are the nth order Bessel functions of first kind and second kind, respectively, while I_n and K_n are the nth order modified Bessel functions of first kind and second kind, respectively, c_i–c_4 are integration constants determined by the boundary conditions, and

$$z = 2\beta\xi^{1/2}, \tag{9}$$

$$\beta^4 = \omega^2 L_1^4\left(\frac{\rho A_1}{EI_1}\right). \tag{10a}$$

Substituting the values of A_1 and I_1 defined by Eq. (8) into Eq. (10a), one obtains

$$\beta_r^2 = \frac{\omega_r L_1^2}{h_1}\sqrt{\frac{12\rho}{E}}. \tag{10b}$$

For the single-tapered beam as shown in Fig. 1, the width is constant and the depth is linearly varying, i.e.,

$$b(\xi) = b_1 = b_0 = constant, \tag{11}$$

$$h(\xi) = \alpha\xi L_1 \tag{12}$$

with

$$\alpha = h_1/L_1 = h_0/L_0, \tag{13}$$

$$\xi_0 = L_0/L_1, \tag{14}$$

where α is the taper ratio.

From Eqs. (5), (8), (11) and (12), one sees that parameter n for single-tapered beam shown in Fig. 1 is equal to one, i.e., $n=1.0$ Hence, Eq. (7) reduces to

$$W(\xi) = L_1^{-1/2}\xi^{-1/2}[c_1\mathrm{J}_1(z) + c_2\mathrm{Y}_1(z) + c_3\mathrm{I}_1(z) + c_4\mathrm{K}_1(z)]. \tag{15}$$

For the free–clamped (FC) single-tapered beam shown in Fig. 1, one has

$$\frac{\mathrm{d}^2W}{\mathrm{d}\xi^2} = \frac{\mathrm{d}}{\mathrm{d}\xi}\left(EI(\xi)\frac{\mathrm{d}^2W}{\mathrm{d}\xi^2}\right) = 0 \quad \text{at} \quad \xi = \xi_0 = L_0/L_1, \tag{16a, b}$$

$$W = \frac{\mathrm{d}W}{\mathrm{d}\xi} = 0 \quad \text{at} \quad \xi = 1.0. \tag{17a, b}$$

The substitution of Eq. (15) into Eqs. (16a), (16b), (17a) and (17b) gives

$$c_1\mathrm{J}_2(z_0) + c_2\mathrm{Y}_2(z_0) + c_3\mathrm{I}_2(z_0) - c_4\mathrm{K}_2(z_0) = 0, \tag{18a}$$

$$c_1\mathrm{J}_3(z_0) + c_2\mathrm{Y}_3(z_0) + c_3\mathrm{I}_3(z_0) + c_4\mathrm{K}_3(z_0) = 0, \tag{18b}$$

$$c_1\mathrm{J}_1(2\beta) + c_2\mathrm{Y}_1(2\beta) + c_3\mathrm{I}_1(2\beta) + c_4\mathrm{K}_1(2\beta) = 0, \tag{18c}$$

$$c_1\mathrm{J}_2(2\beta) + c_2\mathrm{Y}_2(2\beta) - c_3\mathrm{I}_2(2\beta) + c_4\mathrm{K}_2(2\beta) = 0, \tag{18d}$$

where

$$z_0 = 2\beta\xi_0^{1/2} = 2\beta(L_0/L_1)^{1/2}. \tag{19}$$

Non-trivial solution of Eq. (18) requires that

$$\begin{vmatrix} \mathrm{J}_2(z_0) & \mathrm{Y}_2(z_0) & \mathrm{I}_2(z_0) & -\mathrm{K}_2(z_0) \\ \mathrm{J}_3(z_0) & \mathrm{Y}_3(z_0) & \mathrm{I}_3(z_0) & \mathrm{K}_3(z_0) \\ \mathrm{J}_1(2\beta) & \mathrm{Y}_1(2\beta) & \mathrm{I}_1(2\beta) & \mathrm{K}_1(2\beta) \\ \mathrm{J}_2(2\beta) & \mathrm{Y}_2(2\beta) & -\mathrm{I}_2(2\beta) & \mathrm{K}_2(2\beta) \end{vmatrix} = 0. \tag{20}$$

From the last equation one may determine the values of $\beta = \beta_r$ ($r = 1,2,3,\ldots$). The associated values of $\omega = \omega_r$ obtained from Eq. (10) are the corresponding natural frequencies, i.e.,

$$\omega_r = \left(\frac{\beta_r}{L_1}\right)^2\sqrt{\frac{EI_1}{\rho A_1}} \quad (r = 1, 2, 3, \ldots). \tag{21}$$

The corresponding mode shapes may be obtained from Eq. (15), i.e.,

$$W_r(\xi) = L_1^{-1/2}\xi^{-1/2}[c_1\mathrm{J}_1(z_r) + c_2\mathrm{Y}_1(z_r) + c_3\mathrm{I}_1(z_r) + c_4\mathrm{K}_1(z_r)], \tag{22}$$

where

$$z_r = 2\beta_r\xi^{1/2}. \tag{23}$$

The mode shapes $W(\xi)$ given by Eq. (22) are the natural mode shapes. In order to apply the ANCM to the title problem, one requires to obtain the normal mode shapes $\bar{W}_r(\xi)$. The latter must satisfy the following orthonormal conditions:

$$\int_{\xi_0}^{1} \bar{W}_r(\xi)\rho A(\xi)\bar{W}_s(\xi)L_1 \,\mathrm{d}\xi = \delta_{rs}, \tag{24}$$

where $\xi_0 = L_0/L_1$ and δ_{rs} is the Kronecker's delta.

For the single-tapered beam studied in this paper (see Fig. 1), from Eq. (4a) one has

$$A(\xi) = A_1\xi. \tag{25}$$

From Eqs. (24) and (25) one obtains the normal mode shapes to be

$$\bar{W}_r(\xi) = C_r W_r(\xi), \tag{26}$$

where

$$C_r = \sqrt{\frac{1}{\rho A_1 B_r}}, \tag{27}$$

$$B_r = \int_{\xi_0}^{1} [c_{1r}\mathrm{J}_1(z_r) + c_{2r}\mathrm{Y}_1(z_r) + c_{3r}\mathrm{I}_1(z_r) + c_{4r}\mathrm{K}_1(z_r)]^2 \,\mathrm{d}\xi. \tag{28}$$

The analytical integration of Eq. (28) is usually difficult. In such a case one may obtain the numerical values of B_r ($r = 1,2,3,\ldots$) by means of Simpson's rule. Simpson's rule is one of the techniques for calculating the area under a curve. Because the curves defined by mode shapes of a wedge beam, shown in Eq. (28), are very smooth, one requires only small number of subdivision intervals, n_i, for Simpson's rule. In this paper, $n_i = 80$ was used in numerical integration of Eq. (28). It has been found that differences between natural frequencies based on $n_i = 80$ and those based on $n_i = 160$ are very small and negligible.

Besides the free–clamped (FC) beam described above, the other five boundary conditions of the single-tapered beam are also studied in this paper: HC, CC, CF, CH and HH. (Here H, C and F represent hinged, clamped and free ends, respectively.) For the associated frequency equations, one may refer to Refs. [14,29,30].

3. Natural frequencies and mode shapes of the constrained wedge beams

For a non-uniform Euler–Bernoulli beam carrying P point masses with magnitudes m_j ($j = 1-\mathrm{P}$) located at x_j, the equation of motion is given by (see Fig. 2)

$$\frac{\partial^2}{\partial x^2}\left(EI(x)\frac{\partial^2 y(x,t)}{\partial x^2}\right) + \rho A(x)\frac{\partial^2 y(x,t)}{\partial t^2} = -\sum_{j=1}^{P} m_j \frac{\partial^2 y(x,t)}{\partial t^2}\delta(x - x_j), \tag{29}$$

where $\delta(\cdot)$ denotes the Dirac delta function and meanings of the other symbols are exactly the same as in Eq. (1).

According to the method of separation of variables and the expansion theorem [32,33], we set

$$y(x,t) = \sum_{s=1}^{\bar{n}} \bar{W}_s(x)\eta_s(t), \tag{30}$$

where $\bar{W}_s(x)$ is the sth normal mode shape of the unconstrained beam obtained in the last section, $\eta_s(t)$ is the associated generalized co-ordinate and $\bar{n}$ is the total number of modes considered.

Substituting Eq. (30) into Eq. (29), multiplying the resulting expression by $\bar{W}_r(x)\,dx$, then integrating each term over the whole length of the beam (i.e., $x = L_0 - L_1$) and using the orthogonal property between normal mode shapes, one obtains

$$M_{rr}\ddot{\eta}_r(t) + K_{rr}\eta_r(t) = N_{rr}(t), \tag{31}$$

where M_{rr}, K_{rr} and N_{rr} represent the generalized mass, generalized stiffness and generalized force, respectively, and are given by

$$M_{rr} = \int_{\xi_0}^{1} \bar{W}_r(\xi)\rho A(\xi)\bar{W}_r(\xi)L_1\,d\xi, \tag{32a}$$

$$K_{rr} = \left(\frac{1}{L_1^3}\right)\int_{\xi_0}^{1} \bar{W}_r(\xi)\left[\frac{\partial^2}{\partial\xi^2}\left(EI(\xi)\frac{\partial^2\bar{W}_r(\xi)}{\partial\xi^2}\right)\right]d\xi, \tag{32b}$$

$$N_{rr} = -\sum_{j=1}^{P}\sum_{s=1}^{\bar{n}} m_j\bar{W}_r(\xi_j)\bar{W}_s(\xi_j)\ddot{\eta}_s(t), \tag{32c}$$

where

$$\bar{W}_r(\xi_j) = \bar{W}_r(\xi)\cdot\delta(\xi-\xi_j), \quad \xi_j = x_j/L_1. \tag{33a, b}$$

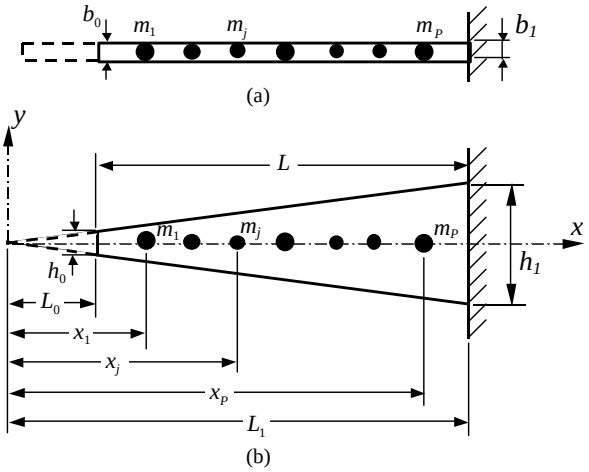

Fig. 2. A free–clamped (FC) single-tapered beam carrying P point masses m_j located at $\xi_j = x_j/L_1$ ($j = 1$–P): (a) top view; (b) front view.

From Eq. (24) one sees that $M_{rr} = 1.0$. Thus Eq. (31) reduces to

$$\ddot{\eta}_r(t) + \omega_r^2 \eta_r(t) = N_{rr}(t), \tag{34}$$

where

$$\omega_r = \sqrt{K_{rr}/M_{rr}} \tag{35}$$

which is the natural frequency of the unconstrained beam.

When the constrained beam performs free vibration with frequency $\bar{\omega}$, one has

$$\eta_r(t) = \bar{\eta}_r e^{i\bar{\omega}t}, \tag{36}$$

where $\bar{\eta}_r$ represents the amplitude of $\eta_r(t)$. Substituting Eq. (36) in Eq. (32c), then inserting the result into Eq. (34), one obtains

$$\left(\omega_r^2 - \bar{\omega}^2\right)\bar{\eta}_r - \bar{\omega}^2 \sum_{j=1}^{P} \sum_{s=1}^{\bar{n}} m_j \bar{W}_r(\xi_j) \bar{W}_s(\xi_j) \bar{\eta}_r = 0 \quad (r = 1 - \bar{n}) \tag{37}$$

or in matrix form we have

$$\begin{bmatrix} \ddots & & \\ & \omega^2 & \\ & & \ddots \end{bmatrix} \{\bar{\eta}\} - ([I] + [\bar{B}])\bar{\omega}^2 \{\bar{\eta}\} = 0, \tag{38}$$

where

$$\begin{bmatrix} \ddots & & \\ & \omega^2 & \\ & & \ddots \end{bmatrix} = \lceil\, \omega_1^2 \quad \omega_2^2 \quad \omega_3^2 \quad \ldots \quad \omega_{\bar{n}}^2 \,\rfloor, \tag{39a}$$

$$\begin{bmatrix} \ddots & & \\ & I & \\ & & \ddots \end{bmatrix} = \lceil\, 1 \quad 1 \quad 1 \quad \ldots \quad 1 \,\rfloor, \tag{39b}$$

$$[\bar{B}] = \sum_{j=1}^{P} m_j \{\bar{W}(\xi_j)\} \{\bar{W}(\xi_j)\}^{\mathrm{T}}, \tag{39c}$$

$$\{\bar{W}(\xi_j)\} = \{\bar{W}_1(\xi_j) \quad \bar{W}_2(\xi_j) \quad \ldots \quad \bar{W}_{\bar{n}}(\xi_j)\}, \tag{39d}$$

$$\{\bar{\eta}\} = \{\bar{\eta}_1 \quad \bar{\eta}_2 \quad \ldots \quad \bar{\eta}_{\bar{n}}\}. \tag{39e}$$

In the foregoing equations, the symbols $\lceil\ \rfloor$, $[\,]$ and $\{\,\}$ represent the diagonal matrix, square matrix and column vector, respectively.

For convenience, Eq. (38) is further rewritten as

$$\left(\begin{bmatrix} \ddots & & \\ & \omega^2 & \\ & & \ddots \end{bmatrix} - \bar{\omega}^2 [B] \right) \{\bar{\eta}\} = 0, \tag{40}$$

where

$$[B] = \begin{bmatrix} \diagdown & & \\ & I & \\ & & \diagdown \end{bmatrix} + [\bar{B}]. \tag{41}$$

Eq. (40) is a standard characteristic equation. One may use the Jacobi method [34] to determine the eigenvalues $\bar{\omega}_s$ and the corresponding eigenvectors $\{\bar{\eta}\}^{(s)}$, where $\bar{\omega}_s$ is the sth natural frequency of the constrained beam (carrying any point masses) and the corresponding sth mode shape is determined by

$$\tilde{W}_s(\xi) = \{\bar{W}(\xi)\}^{\mathrm{T}}\{\bar{\eta}\}^{(s)} \quad (s = 1-\bar{n}). \tag{42}$$

4. Numerical results and discussions

Physical properties and dimensions of the single-tapered beam (see Fig. 1) studied are: Young's modulus $E = 2.051 \times 10^{11}\,\mathrm{N/m^2}$, mass density $\rho = 7850\,\mathrm{kg/m^3}$, beam width $b_1 = b_0 = 0.1\,\mathrm{m}$, beam depth at large end $h_1 = 0.4\,\mathrm{m}$, distance from origin to large end of beam $L_1 = 2.0\,\mathrm{m}$, distance from origin to small end of beam $L_0 = 0.4\,\mathrm{m}$ (excluding Table 1). In order to validate the numerical results obtained from the present method (ANCM), each example was also calculated using the finite element method (FEM) [35]. To this end, the tapered beam was replaced by an equivalent stepped beam composed of 80 uniform beam elements as shown in Fig. 3 and the total number of modes considered by ANCM is $\bar{n} = 6$. In general, the accuracy of the lowest $\bar{n} - 1$ natural frequencies and mode shapes of the constrained beam is reasonable for ANCM as shown in Ref. [27].

4.1. Comparison with the existing literature

The presented theory is available for the beams carrying any number of point masses, P. Therefore, the ANCM results for the free–clamped (FC) single-tapered beams carrying no attachments (i.e., $P = 0$) will agree with those of the unconstrained cantilever beams of Ref. [2]. Table 1 shows the values of the parameter β_r^2 obtained from present paper and those from Ref. [2] for the cases of $L_1/L_0 = 2, 3, 4, 10$ (here $L_1 = 2.0\,\mathrm{m} = \textit{constant}$). In Ref. [2], $A = (h_1/2)/L_1$ and $p = \omega$. Thus substitution of the last relationship into the expression $\xi = q_2 L_1 = (pL_1/A)\sqrt{3\rho/E}$ (see Fig. 1 and Table 4 of Ref. [2]) will yield identical equation for β_r^2 defined by Eq. (10b) of this paper. From Table 1 one sees that the values of β_r^2 obtained from the present paper are in good agreement with those of Ref. [2].

4.2. Influence of number of finite elements on the natural frequencies

To determine the natural frequencies of a non-uniform beam by conventional FEM, one requires to replace the original beam (see Fig. 1) by the equivalent stepped beam (see Fig. 3) composed of a number of uniform beam segments (or finite elements). Table 2 gives the natural frequencies of the free–clamped (FC) single-tapered beam shown in Fig. 1 with $L_0 = 0.4\,\mathrm{m}$ for the

Table 1
Comparison for the values of β_r^2 obtained from present paper and Ref. [2]

L_1/L_0	Methods	β_1^2	β_2^2	β_3^2	β_4^2	β_5^2
2	Present	15.295	73.269	189.059	361.802	592.007
	Ref. [2]	15.3[a]	73.3	189.0	362.0	592.0
3	Present	9.061	38.062	93.959	177.083	287.731
	Ref. [2]	9.06	38.1	94.0	177.0	288.0
4	Present	7.425	28.772	68.933	128.455	207.591
	Ref. [2]	7.43	28.8	68.9	128.0	208.0
10	Present	5.717	18.433	40.535	72.737	115.294
	Ref. [2]	5.72	18.4	40.5	72.7	115.0

[a] All numerical values given by Ref. [2] have only three digits.

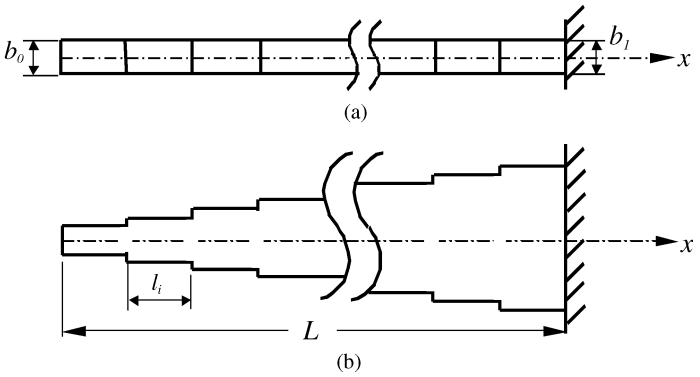

Fig. 3. The finite element model for the free–clamped (FC) single-tapered beam studied: (a) top view; (b) front view.

cases of number of finite elements (N_e =)16, 32, 48, 64, 80. Table 2(a) is for the unconstrained beam with no attachment (i.e., $P = 0$), while Tables 2(b) and (c) are, respectively, for the constrained beams carrying one point mass ($P = 1$ with magnitude $m_1 = m_b/5 = 60.288$ kg located at $\xi_1 = x_1/L_1 = L_0/L_1 = 0.2$, where $m_b = 301.44$ kg is the total mass of the tapered beam) and five point masses ($P = 5$ with magnitudes $m_j = m_b/5 = 60.288$ kg located at $\xi_j = x_j/L_1 = 0.3, 0.45, 0.6, 0.75, 0.9$; $j = 1-5$). From Tables 2(a)–(c) one sees that either the lowest five natural frequencies of the unconstrained beam (ω_1–ω_5) or those of the constrained beams ($\bar{\omega}_1 - \bar{\omega}_5$) increase with increasing the number of finite elements N_e and approach constants for N_e greater than 80. Therefore, the subsequent FEM results are based on $N_e = 80$. It is noted that one must calculate the cross-sectional area (A) and moment of inertia (I) of each finite beam element from the width and depth of the corresponding "uniform" beam segment (Fig. 3) and must not directly take the mean values of A's and I's from the associated "non-uniform" beam segment (Fig. 1).

4.3. Natural frequencies and mode shapes of the free–clamped (FC) beam

To show the effectiveness of the presented theory, the free–clamped (FC) single-tapered beam shown in Fig. 2 ($L_0 = 0.4$ m) with $P = 0$ (no attachment), $P = 1$ (one point mass attached) and

Table 2
Influence of element number (N_e) on the lowest five natural frequencies of the FC single-tapered beam carrying P point masses using FEM: (a) $P = 0$; (b) $P = 1$ (with $m_1 = m_b/5 = 60.288$ kg located at $\xi_1 = x_1/L_1 = L_0/L_1 = 0.2$); (c) $P = 5$ (with $m_j = m_b/5 = 60.288$ kg located at $\xi_j = x_j/L_1 = 0.3, 0.45, 0.6, 0.75, 0.9$; $j = 1$–5)

Number of elements, N_e	Natural frequencies, ω_i (rad/s)				
	ω_1	ω_2	ω_3	ω_4	ω_5
(a) $P = 0$					
16	985.6516	3606.0146	8439.5203	15581.7720	25075.8849
32	988.6574	3623.6492	8487.5440	15672.5252	25214.9764
48	989.2355	3627.0143	8496.8141	15690.5746	25244.2108
64	989.4102	3628.0938	8499.8388	15696.5316	25254.0097
80	989.5017	3628.6311	8501.3310	15699.4691	25258.8597
	Natural frequencies, $\bar{\omega}_i$ (rad/s)				
	$\bar{\omega}_1$	$\bar{\omega}_2$	$\bar{\omega}_3$	$\bar{\omega}_4$	$\bar{\omega}_5$
(b) $P = 1$					
16	567.5976	2493.1872	6679.4115	13226.7517	22140.6722
32	568.9315	2501.1023	6702.6176	13273.3556	22214.4561
48	569.1872	2502.6033	6707.0080	13282.3127	22229.4133
64	569.2638	2503.0602	6708.3547	13285.0782	22234.0869
80	569.3039	2503.2976	6709.0488	13286.4974	22236.4917
(c) $P = 5$					
16	611.4682	2513.3925	6318.6153	11965.3103	15732.6558
32	612.7602	2521.9491	6345.8905	12075.1412	15852.0428
48	613.0102	2523.5738	6351.0350	12095.7223	15874.1878
64	613.0835	2524.0820	6352.6796	12102.6284	15881.5535
80	613.1226	2524.3389	6353.4962	12105.9359	15885.0965

$P = 5$ (five point masses attached) are investigated. The magnitudes and locations of the point masses are exactly the same as those shown in Table 2. Table 3 and Fig. 4 show the lowest five natural frequencies and the associated mode shapes of the cantilever beam obtained from ANCM and FEM, respectively. From Table 3 one finds that FEM results are very close to ANCM results. The percentage differences shown in the final rows of Tables 3(a)–(c) are calculated with the formula $Difference = (\omega_{i,ANCM} - \omega_{i,FEM}) \times 100\%/\omega_{i,ANCM}$ for $i = 1$–5 where $\omega_{i,ANCM}$ and $\omega_{i,FEM}$ denote the i-th natural frequencies obtained from ANCM and FEM, respectively. It has been shown in Ref. [36] that the accuracy of ANCM is better than that of FEM. This will be the reason why the values of $\bar{\omega}_{i,ANCM}$ (or $\omega_{i,ANCM}$) are greater than the corresponding ones of $\bar{\omega}_{i,FEM}$ (or $\omega_{i,FEM}$) in Table 3. In other words, the values of $\bar{\omega}_{i,FEM}$ (or $\omega_{i,FEM}$) will approach the corresponding ones of $\bar{\omega}_{i,ANCM}$ (or $\omega_{i,ANCM}$) when the number of finite elements (N_e) increases gradually according to the result of the last subsection. Although the magnitude of the single-point mass for Table 3(b) is only one-fifth of the total point masses for Table 3(c), the lowest two natural frequencies of the cantilever beam carrying a tip mass are lower than the corresponding ones of the same beam carrying five uniformly distributed point masses. This means that the effect

Table 3
Comparison between the lowest five natural frequencies obtained from the ANCM and those from the FEM: (a) $P = 0$; (b) $P = 1$; (c) $P = 5$

Methods	Natural frequencies, ω_i (rad/s)					CPU time
	ω_1	ω_2	ω_3	ω_4	ω_5	(s)
(a) $P = 0$						
ANCM	989.6626	3629.5821	8503.9741	15704.6849	25267.5120	1
FEM	989.5017	3628.6311	8501.3310	15699.4691	25258.8597	13
Difference	0.016%	0.026%	0.031%	0.033%	0.034%	—
	Natural frequencies, $\bar{\omega}_i$ (rad/s)					CPU time
	$\bar{\omega}_1$	$\bar{\omega}_2$	$\bar{\omega}_3$	$\bar{\omega}_4$	$\bar{\omega}_5$	(s)
(b) $P = 1$						
ANCM	569.6273	2508.8947	6743.2318	13408.5313	22570.1693	1
FEM	569.3039	2503.2976	6709.0487	13286.4974	22236.4917	13
Difference[a]	0.057%	0.223%	0.507%	0.910%	1.478%	—
(c) $P = 5$						
ANCM	613.2201	2525.5381	6366.4999	12184.0282	16089.9494	1
FEM	613.1226	2524.3389	6353.4962	12105.9359	15885.0965	13
Difference[a]	0.016%	0.047%	0.204%	0.641%	1.273%	—

The magnitudes and locations of the point masses are the same as those shown in Table 2.
[a] *Difference*$=(\omega_{i,ANCM}-\omega_{i,FEM}) \times 100\%/\omega_{i,ANCM}$.

of distribution of the attached point masses along the beam length must be considered in addition to the effect of the magnitudes of the point masses. From Table 3 one sees that the CPU time (for PC Pentium II) required by FEM is about 13 times that required by ANCM.

From Fig. 4 one sees that the dashed curves obtained from FEM are well coincident with the corresponding dotted curves obtained from ANCM. Furthermore, the profile of 1st to 4th mode shapes for the unconstrained beam shown in Figs. 4(a) and (a)′ agree with that shown in Ref. [7, Fig. 4]. In addition, for a clamped–free torsional shaft carrying a rigid disk at the free end, the rigid disk will asymptotically approach zero deflection for the higher mode shapes [33,36]. This is the reason why the mode displacement of the tip mass (at left end of the beam) decreases with increase of mode number as shown in Figs. 4(b) and (b)′ for the bending cantilever beam with one point mass at the free end. From Fig. 4 one also finds that the lowest five mode shapes for the tapered beam carrying five point masses (Figs. 4(c) and (c)′) look like those for the unconstrained beam (without any attachment, Figs. 4(a) and (a)′). This is because the five point masses are identical and uniformly distributed along the beam length.

4.4. Natural frequencies of the constrained beam carrying five point masses in six end conditions

In this subsection, the lowest five natural frequencies of the constrained beam carrying five identical point masses ($P = 5$) with six end conditions are investigated (see Fig. 2). The

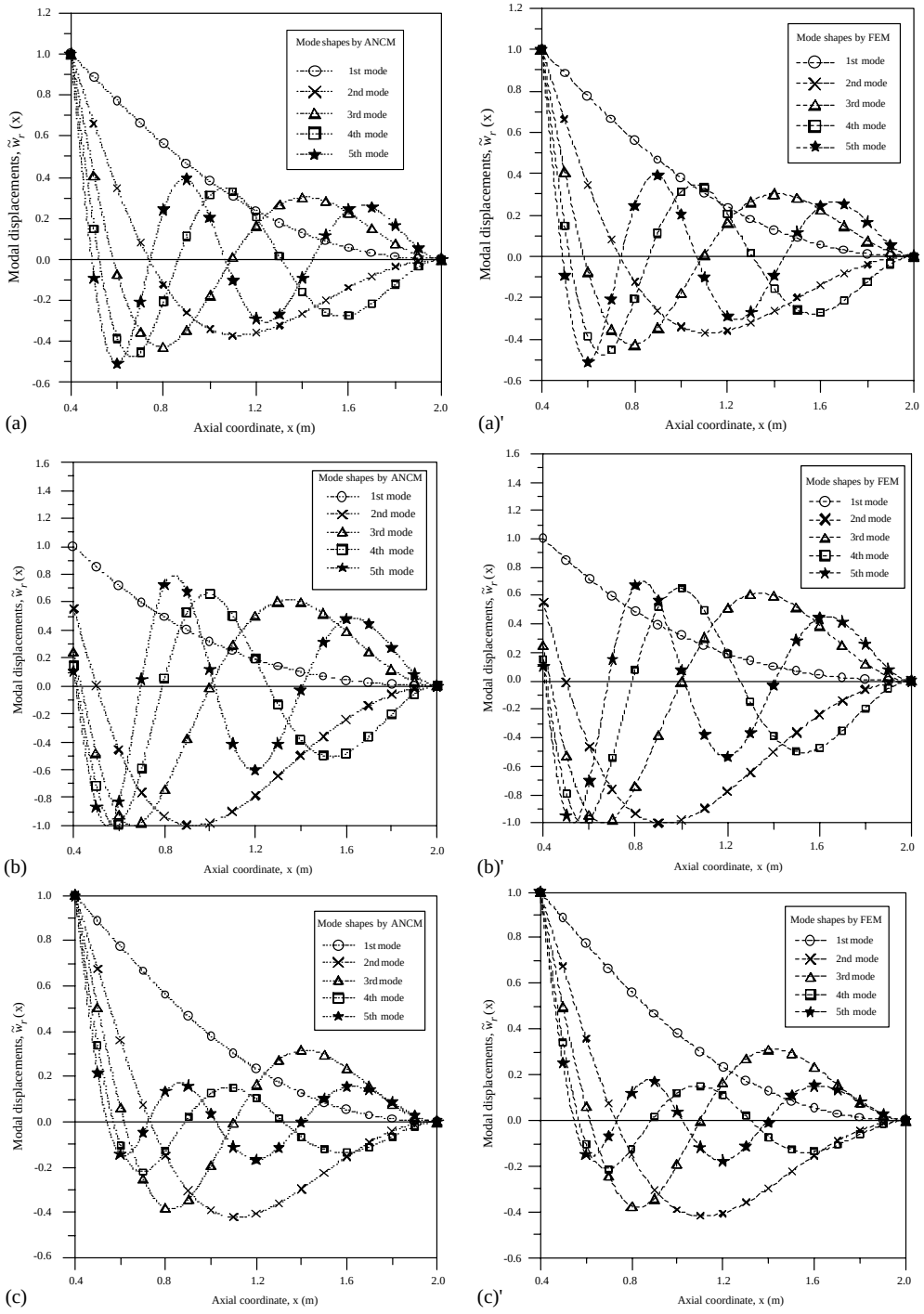

Fig. 4. The lowest five mode shapes of the free–clamped (FC) wedge beam carrying P point masses obtained from ANCM (⋯⋯) and those from FEM (— — —) for (a), (a)′ $P = 0$; (b), (b)′ $P = 1$; (c), (c)′ $P = 5$; while ○, ×, △, □, and ★ are for the 1st, 2nd, 3rd, 4th and 5th mode shapes, respectively.

magnitudes and locations of the five point masses are exactly the same as those shown in Table 2, i.e., $m_j = m_b/5 = 60.288$ kg and $\xi_j = x_j/L_1 = 0.3, 0.45, 0.6, 0.75, 0.9$ ($j = 1-5$). In addition to the free–clamped (FC) beam shown in Figs. 1–3, the other five end conditions of the beam are hinged–clamped (HC), clamped–clamped (CC), clamped–free (CF), clamped–hinged (CH) and hinged–hinged (HH). The frequency equations for the associated unconstrained beams can be found from Refs. [14,29,30]. From the frequency equations and Eq. (21) one may determine the natural frequencies of the unconstrained beams and referring to Eqs. (22) and (26) one may obtain the associated normal mode shapes. Finally, the natural frequencies and mode shapes of the constrained beams are determined by means of Eqs. (40) and (42).

From Table 4 one sees that the lowest five natural frequencies of the constrained beams obtained from ANCM, $\bar{\omega}_{i,ANCM}$ ($i = 1$–4), and those obtained from FEM, $\bar{\omega}_{i,FEM}$ ($i = 1$–4), are in good agreement in every end condition. The influence of the end conditions on the lowest five natural frequencies is $\bar{\omega}_{i,CC} > \bar{\omega}_{i,HC} > \bar{\omega}_{i,CH} > \bar{\omega}_{i,HH} > \bar{\omega}_{i,FC} > \bar{\omega}_{i,CF}$. It is evident that the last relationship holds only if the beam is positively tapered (i.e., the left end is smaller and the right end is larger, as shown in Figs. 1–3); for a negatively tapered beam (with left end larger and right end smaller) the last relationship should be changed to $\bar{\omega}_{i,CC} > \bar{\omega}_{i,CH} > \bar{\omega}_{i,HC} > \bar{\omega}_{i,HH} > \bar{\omega}_{i,CF} > \bar{\omega}_{i,FC}$.

From Table 4 one also sees that the values of $\bar{\omega}_{i,ANCM}$ are greater than the corresponding ones of $\bar{\omega}_{i,FEM}$ with very few exceptions. This agrees with the results for the FC beam studied in the previous subsections (see Table 3). As to the few exceptions, they may have something to do with accuracy of numerical computations, convergent tolerance for Jacobi method, or step sizes for the cut and try numerical approaches.

4.5. *Influence of truncated ratio on the natural frequencies of the FC wedge beam carrying 10 point masses*

As shown in Figs. 1 and 2, if L_0 and L_1 represent the distances from the tip of the "complete" wedge beam to the small and large ends of the corresponding "truncated" tapered beam, respectively, then the ratio $R_t = L_0/L_1$ is called the "truncated ratio" in this paper. The objective of this subsection is to investigate the influence of the truncated ratio (R_t) on the lowest five natural frequencies of the foregoing tapered beam. The dimensions and the physical properties of the beam are the same as the last examples except that the values of L_0 are 0.05, 0.20 and 0.40 m (corresponding to the truncated ratios ($R_t = L_0/L_1 =$) 0.025, 0.1 and 0.2), respectively. For simplicity, only the free–clamped (FC) beam carrying ten ($P = 10$) uniformly distributed point masses with identical magnitude $m_j = m_b/10 = 30.144$ kg ($j = 1$–10) is studied. The spacing between any two adjacent point masses is $\Delta x_j = (L_1 - L_0)/10$ ($j = 1$–10) and one of the point masses is located at the free end (with smallest cross-sectional area). The results as shown in Table 5 are obtained using 80 beam elements (i.e., $N_e = 80$) for FEM and 80 integration intervals (i.e., $n_i = 80$) for ANCM. From Table 5 one sees that the lowest two natural frequencies obtained from FEM are very close to the corresponding ones obtained from ANCM for the cases of truncated ratios ($R_t = L_0/L_1 =$) 0.025, 0.1 and 0.2. The percentage difference between the natural frequencies obtained from FEM and ANCM decreases with increase in the truncated ratio R_t and for the case of $R_t = 0.2$, the biggest percentage difference is smaller than 0.039% for the first natural frequency and 1.374% for the fifth natural frequency. It is noted that the

Table 4
The lowest five natural frequencies obtained from the ANCM and those from the FEM for the single-tapered beam carrying five point masses ($P = 5$) with six kinds of boundary conditions

Boundary conditions	Methods	Natural frequencies, $\bar{\omega}_i$ (rad/s)				
		$\bar{\omega}_1$	$\bar{\omega}_2$	$\bar{\omega}_3$	$\bar{\omega}_4$	$\bar{\omega}_5$
FC	ANCM	613.2201	2525.5381	6366.4999	12184.0282	16089.9494
	FEM	613.1226	2524.3389	6353.4962	12105.9359	15885.0965
	Difference[a]	0.016%	0.047%	0.204%	0.641%	1.273%
HC	ANCM	1459.1106	4105.9737	8025.0232	14581.7560	30488.5776
	FEM	1458.6114	4097.4309	7985.8453	14526.3489	29897.8784
	Difference[a]	0.034%	0.208%	0.488%	0.380%	1.937%
CC	ANCM	1810.1240	4855.3673	8800.2959	14819.6266	31073.3722
	FEM	1810.4456	4849.3983	8753.7178	14759.7359	30383.5348
	Difference[a]	−0.018%	0.123%	0.529%	0.404%	2.220%
CF	ANCM	108.5195	1391.2900	4610.2500	8680.4611	15088.1528
	FEM	108.5848	1391.7859	4602.9112	8630.0374	14786.3576
	Difference[a]	−0.060%	−0.036%	0.159%	0.581%	2.000%
CH	ANCM	1014.3480	3781.0366	7595.8442	12630.1757	23820.1082
	FEM	1014.7597	3778.8431	7565.2554	12540.7835	23627.7206
	Difference[a]	−0.041%	0.058%	0.403%	0.708%	0.808%
HH	ANCM	765.6113	3140.2938	6724.8871	12257.9200	23774.0557
	FEM	765.4745	3136.4515	6691.3136	12184.5714	23493.7720
	Difference[a]	0.018%	0.122%	0.499%	0.598%	1.179%

The magnitudes and locations of the point masses are the same as those shown in Table 2.
[a] $Difference = (\bar{\omega}_{i,ANCM} - \bar{\omega}_{i,FEM}) \times 100\%/\bar{\omega}_{i,ANCM}$.

above-mentioned percentage differences were determined by means of the formula $Difference = (\bar{\omega}_{i,ANCM} - \bar{\omega}_{i,FEM}) \times 100\%/\bar{\omega}_{i,ANCM}$.

In theory, the formulation of this paper is available for the cases with small truncated ratio (i.e., $R_t \approx 0$). Therefore, the reason why the percentage difference becomes larger for very small value of R_t requires further study.

5. Conclusions

1. For a wedge beam carrying multiple point masses along the beam length, the lowest i-th natural frequencies and the corresponding mode shapes determined by ANCM are very close to those by FEM if $i < (\bar{n} - 1)$, where $\bar{n}$ is the total number of natural frequencies and mode shapes of the associated unconstrained beam considered by ANCM.
2. If $\bar{\omega}_i$ denotes the ith natural frequency of a wedge beam carrying uniformly distributed point masses, then the influence of end conditions on the lowest five natural frequencies is $\bar{\omega}_{i,CC} >$

Table 5
Influence of truncated ratio ($R_t = L_0/L_1$) on the lowest five natural frequencies of the FC wedge beam carrying 10 point masses ($P = 10$) uniformly distributed along the beam length with one point mass at free end ($L_1 = 2.0\,\text{m}$, $\Delta x_j = (L_1 - L_0)/10$, $m_j = m_b/10 = 30.144\,\text{kg}$, $j = 1$–10, $N_e = n_i = 80$)

Truncated ratios $R_t = L_0/L_1$	Methods	Natural frequencies, $\bar{\omega}_i$ (rad/s)				
		$\bar{\omega}_1$	$\bar{\omega}_2$	$\bar{\omega}_3$	$\bar{\omega}_4$	$\bar{\omega}_5$
0.025	ANCM	317.5752	867.6575	1889.8407	3440.7726	5890.6598
($L_0 = 0.05\,\text{m}$)	FEM	316.5570	850.7947	1803.7740	3251.9752	5625.7222
	Difference[a]	(0.321%)	(1.943%)	(4.554%)	(5.487%)	(4.498%)
0.1	ANCM	542.3880	1807.4390	4601.3575	8997.0833	15030.104
($L_0 = 0.2\,\text{m}$)	FEM	541.7439	1800.2370	4567.4171	8889.6911	14756.549
	Difference[a]	(0.119%)	(0.398%)	(0.738%)	(1.194%)	(1.820%)
0.2	ANCM	702.4768	2687.1889	6909.4343	13557.796	22700.479
($L_0 = 0.4\,\text{m}$)	FEM	702.2051	2682.3347	6878.7073	13445.516	22388.680
	Difference[a]	(0.039%)	(0.181%)	(0.445%)	(0.828%)	(1.374%)

[a] $\textit{Difference} = (\bar{\omega}_{i,ANCM} - \bar{\omega}_{i,FEM}) \times 100\% \,/\bar{\omega}_{i,ANCM}$.

$\bar{\omega}_{i,HC} > \bar{\omega}_{i,CH} > \bar{\omega}_{i,HH} > \bar{\omega}_{i,FC} > \bar{\omega}_{i,CF}$ for the positively tapered beam (with left end smaller and right end larger). However, for the negatively tapered beam (with left end larger and right end smaller) the last relationship should be changed to $\bar{\omega}_{i,CC} > \bar{\omega}_{i,CH} > \bar{\omega}_{i,HC} > \bar{\omega}_{i,HH} > \bar{\omega}_{i,CF} > \bar{\omega}_{i,FC}$, where the subscripts C, H and F denote the clamped, hinged and free ends, respectively.

3. In addition to the magnitudes of the point masses, the distribution of the point masses along the length of the beam affects the dynamic behavior of the beam significantly.
4. For a cantilever beam carrying a point mass at the free end, the point mass will asymptotically approach zero deflection at higher modes.
5. For the examples illustrated in this paper, reasonable accuracy for the lowest five natural frequencies and the corresponding mode shapes can be achieved using 80 beam elements (i.e., $N_e = 80$) for FEM and 80 integration intervals (i.e., $n_i = 80$) for the Simpson's rule.
6. If the truncated ratio for a wedge beam is defined by $R_t = L_0/L_1$, where L_0 and L_1, respectively, denote the distances from the tip of the "complete" wedge beam to the smallest and largest ends of the corresponding "truncated" wedge beam, then for the wedge beam with $R_t > 0.2$, the natural frequencies obtained from FEM are very close to the corresponding ones obtained from ANCM. However, the last conclusion is not necessarily true for the same wedge beam with small truncated ratio (e.g., $R_t < 0.025$). The reasons relating to the last phenomenon require further study.

References

[1] E.T. Cranch, A.A. Adler, Bending vibration of variable section beams, Journal of Applied Mechanics, American Society of Mechanical Engineers 23 (1) (1956) 103–108.

[2] H.D. Conway, J.F. Dubil, Vibration frequencies of truncated-cone and wedge beams, Journal of Applied Mechanics, American Society of Mechanical Engineers 32 (4) (1965) 932–934.

[3] R.P. Goel, Transverse vibration of tapered beams, Journal of Sound and Vibration 47 (1) (1976) 1–7.
[4] G.W. Housner, W.O. Keightley, Vibration of linearly tapered cantilever beams, Journal of the Engineering Mechanics Division, Proceedings of the American Society of Civil Engineers 88 (EM2) (1962) 95–123.
[5] A.C. Heidebrecht, Vibration of non-uniform simply supported beams, Journal of the Engineering Mechanics Division, Proceedings of the American Society of Civil Engineers 93 (EM2) (1967) 1–15.
[6] H.H. Mabie, C.B. Rogers, Transverse vibration of double-tapered cantilever beams, The Journal of the Acoustical Society of America 51 (5 part 2) (1972) 1771–1775.
[7] B. Downs, Transverse vibration of cantilever beams having unequal breadth and depth tapers, Journal of Applied Mechanics, American Society of Mechanical Engineers 44 (4) (1977) 737–742.
[8] C.D. Bailey, Direct analytical solution to non-uniform beam problems, Journal of Sound and Vibration 56 (4) (1978) 501–507.
[9] A.K. Gupta, Vibration of tapered beams, Journal of Structural Engineering 111 (1) (1985) 19–36.
[10] S. Naguleswaran, Vibration of an Euler–Bernoulli beam of constant depth and with linearly varying breadth, Journal of Sound and Vibration 153 (3) (1992) 509–522.
[11] S. Naguleswaran, A direct solution for the transverse vibration of Euler–Bernoulli wedge and cone beams, Journal of Sound and Vibration 172 (3) (1994) 289–304.
[12] S. Abrate, Vibration of non-uniform rods and beams, Journal of Sound and Vibration 185 (4) (1995) 703–716.
[13] P.A.A. Laura, R.H. Gutierrez, R.E. Rossi, Free vibration of beams of bi-linearly varying thickness, Ocean Engineering 23 (1) (1996) 1–6.
[14] A.K. Datta, S.N. Sil, An analysis of free undamped vibration of beams of varying cross-section, Computers and Structures 59 (3) (1996) 479–483.
[15] J.A. Hoffmann, T. Wertheimer, Cantilever beam vibration, Journal of Sound and Vibration 229 (5) (2000) 1269–1276.
[16] H.H. Mabie, C.B. Rogers, Transverse vibration of tapered cantilever beams with end support, The Journal of the Acoustical Society of America 44 (6) (1968) 1739–1741.
[17] H.H. Mabie, C.B. Rogers, Transverse vibration of double-tapered cantilever beams with end support and with end mass, Journal of the Acoustical Society of America 55 (5) (1974) 986–991.
[18] T.W. Lee, Transverse vibration of a tapered beam carrying a concentrated mass, Journal of Applied Mechanics, American Society of Mechanical Engineers 43 (2) (1976) 366–367.
[19] R.O. Grossi, A. Aranda, Vibration of tapered beams with one end spring hinged and the other end with tip mass, Journal of Sound and Vibration 160 (1) (1993) 175–178.
[20] N.M. Auciello, Transverse vibration of a linearly tapered cantilever beam with tip mass of rotatory inertia and eccentricity, Journal of Sound and Vibration 194 (1) (1996) 25–34.
[21] M.A. De Rosa, N.M. Auciello, Free vibration of tapered beams with flexible ends, Computers and Structures 60 (2) (1996) 197–202.
[22] N.M. Auciello, G. Nole, Vibration of a cantilever tapered beam with varying section properties and carrying a mass at the free end, Journal of Sound and Vibration 214 (1) (1998) 105–119.
[23] W.L. Craver Jr., P. Jampala, Transverse vibration of a linearly tapered cantilever beam with constraining springs, Journal of Sound and Vibration 166 (3) (1993) 521–529.
[24] H. Matsuda, C. Morita, T. Sakiyama, A method for vibration analysis of a tapered Timoshenko beam with constraint at any points and carrying a heavy tip body, Journal of Sound and Vibration 158 (2) (1992) 331–339.
[25] N.M. Auciello, M.J. Maurizi, On the natural vibration of tapered beans with attached inertia elements, Journal of Sound and Vibration 199 (3) (1997) 522–530.
[26] J.S. Wu, M. Hsieh, Free vibration analysis of a non-uniform beam with multiple point masses, Structural Engineering and Mechanics 9 (5) (2000) 449–467.
[27] J.S. Wu, T.L. Lin, Free vibration analysis of a uniform cantilever beam with point masses by an analytical-and-numerical-combined method, Journal of Sound and Vibration 136 (1990) 201–213.
[28] T.V. Karman, M.A. Biot, Mathematical Methods in Engineering, McGraw-Hill, New York, 1940, pp. 64–68.
[29] H.D. Conway, E.C.H. Becker, J.F. Dubil, Vibration frequencies of tapered bars and circle plates, Journal of Applied Mechanics, American Society of Mechanical Engineers 31 (2) (1964) 329–331.

[30] D.J. Sanger, Transverse vibration of a class of non-uniform beams, Journal of Mechanical Engineering Science 10 (2) (1968) 111–120.
[31] G.N. Watson, A Treatise on the Theory of Bessel Functions, Cambridge University Press, Cambridge, 1995.
[32] R.W. Clough, J. Penzien, Dynamic of Structures, McGraw-Hill, New York, 1975.
[33] L. Meirovitch, Analytical Methods in Vibration, Macmillan, London, 1967.
[34] K.J. Bathe, Finite Element Procedures, Prentice-Hall International, New York, 1996.
[35] J.S. Przemieniecki, Theory of Matrix Structural Analysis, Dover Publications, New York, 1968.
[36] J.S. Wu, M. Hsieh, On the torsional vibration of a damped shaft system by using the analytical-and-numerical-combined method, Marine Technology 38 (4) (2001) 250–260.